



Contents lists available at ScienceDirect

# Spectrochimica Acta Part A: Molecular and Biomolecular Spectroscopy

journal homepage: [www.journals.elsevier.com/spectrochimica-acta-part-a-molecular-and-biomolecular-spectroscopy](http://www.journals.elsevier.com/spectrochimica-acta-part-a-molecular-and-biomolecular-spectroscopy)

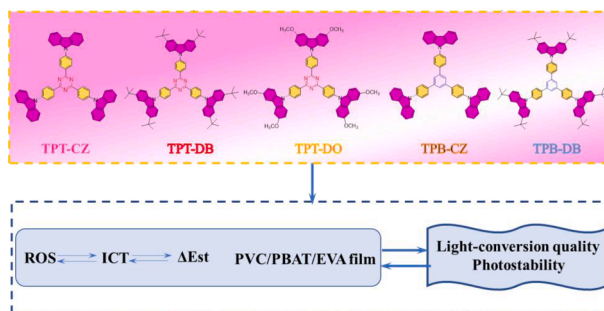
## Breaking the bottleneck of organic light conversion agents: Preparation, performance evaluation and intrinsic mechanism

Yanjin He<sup>a</sup>, Yongtao Wang<sup>a,\*</sup>, Xueming Li<sup>a,\*</sup>, Yanjun Guo<sup>a,\*</sup>, Lei Ma<sup>b</sup><sup>a</sup> Guangxi Key Laboratory of Electrochemical and Magneto-chemical Function Material, College of Chemistry and Bioengineering, Guilin University of Technology, Guilin 541004, China<sup>b</sup> Tianjin International Center for Nanoparticles and Nanosystem, Tianjin University, Tianjin 300072, PR China

## HIGHLIGHTS

- Five dyes with different ICT effect were designed and synthesized.
- TPT-DB shows excellent light conversion performance.
- The factors affecting photostability were analyzed in detail.
- An effective way to improve photostability was obtained.
- The anaerobic environment can enhance photodegradation.

## GRAPHICAL ABSTRACT



## ARTICLE INFO

## Keywords:

Light conversion agent  
Photostability  
Light conversion film  
Triazine derivatives  
Light-conversion quality

## ABSTRACT

Poor photostability has become a major obstacle of organic fluorescent dyes (OFD) used as light conversion agent. To explore the intrinsic mechanisms of photodegradation and highly efficient means to enhance photostability, here, three s-triazine dyes and two 1,3,5-triphenylbenzene luminescent agents were designed and synthesized. Further, the relationships of photostability, intramolecular charge transfer effect, energy gap between singlet and triplet, and active oxygen generating capacity are analyzed and discussed. AIE activity, solid-state fluorescence emission, light conversion quality, and photostability combined with thermostability show TPT-DB (2,4,6-tris(4-(3,6-ditertbutyl-9H-carbazol-9-yl)phenyl)-1,3,5-triazine) is the best light conversion agent among of the dyes, whose photosynthetic photon flux density at 400–500 nm and 600–700 nm in doping film increased successively to 6.20% and 25.78% of the blank film, emission intensity can maintain 93.4% of the initial value after intensified UV radiation of 20 h (365 nm, 40 w), and has good thermal stability, Td up to 374 °C. Furthermore, oxygen-free environment was confirmed to be the most effective measure to enhance the photostability of OFD, thereby a simple and efficient method is adopted to block the diffusion of oxygen and significantly enhance the photostability of OFD by amphiphilic ethylene–vinyl alcohol copolymer. The work not only provides an excellent light conversion agent, but also clears the obstacles for the large-scale application of OFD as light conversion agents.

\* Corresponding authors.

E-mail addresses: [wyt\\_shzu@163.com](mailto:wyt_shzu@163.com) (Y. Wang), [lixueming@glut.edu.cn](mailto:lixueming@glut.edu.cn) (X. Li), [guoyanjun2516@glut.edu.cn](mailto:guoyanjun2516@glut.edu.cn) (Y. Guo).<https://doi.org/10.1016/j.saa.2022.122161>

Received 10 October 2022; Received in revised form 20 November 2022; Accepted 22 November 2022

Available online 26 November 2022

1386-1425/© 2022 Elsevier B.V. All rights reserved.

## 1. Introduction

Currently, functional films have become the main direction of the development of agricultural films. Through wavelength conversion from ultraviolet (290–400 nm) and yellow-green light (510–580 nm) in sunlight to blue-violet light (400–480 nm) and red–orange light (600–700 nm), light conversion agricultural films can increase and improve crop yield and quality, shorten crop growth cycle, and reduce crop diseases and insect pests [1–4]. Furthermore, the properties of light conversion agricultural films mainly depend on absorption and emission spectra, photostability, fluorescence quantum yield (PLQY), and compatibility of light conversion agents with polymer matrices. Among of various light conversion agents, organic fluorescent dyes (OFD) have good resin compatibility, high fluorescence quantum yield and tunable emission wavelengths, meanwhile, OFD used as light conversion agents can promote the sustainable development of agricultural economy by avoiding the use of high-purity rare earth oxides. However, OFD are easy to be bleached and degraded under solar radiation, shortening the service life of light conversion agricultural films, and increasing their application cost. Most importantly, poor photostability has become a major obstacle of the large-scale application for OFD in the field of light conversion agricultural film. Therefore, it is urgent to exploit photostable OFD used as light conversion agents, as well as explore efficient means to enhance photostability and the intrinsic mechanism of photobleaching and photodegradation.

Photobleaching and photodegradation channels of OFD are diverse, and many corresponding details remain unexplored [5–6]. Even so, the existing research results indicate structural modification is still the most straightforward and effective method to enhance the photostability of organic small molecule fluorophores. As we know that chlorophyll is prone to photooxidative degradation, but copper chlorophyll shows significantly enhanced photostability when magnesium atom in porphyrin ring is replaced by copper ion [7]. Our research group found that reducing electron cloud density of the active site can enhance photostability of OFD by introducing electron-withdrawing group [8–9]. More importantly, these approaches have wide applicability rather than individual cases. An early example was a coumarin laser dye, whose photostability was significantly improved by replacing CH<sub>3</sub> group with CF<sub>3</sub> group [10–11] and similar results were also reported by Moi [12] and Zhang [13]. Notably, OFD incorporated electron-withdrawing groups still cannot withstand long-term sunlight radiation.

The photobleaching mechanisms of OFD indicate that the majority of known photobleaching pathways involve high oxidation-active singlet oxygen (<sup>1</sup>O<sub>2</sub>) [11,14–17]. Upon absorbing photon energy, fluorophores transition to the first singlet-excited state (S<sub>1</sub>) from ground state (S<sub>0</sub>). Provided there is a large spin–orbit coupling or small energy gap ( $\Delta E_{st}$ ) between singlet-excited state and triplet-excited state, S<sub>1</sub> can reach triplet-excited state T<sub>n</sub> (n > 1) with different spin multiplicity through

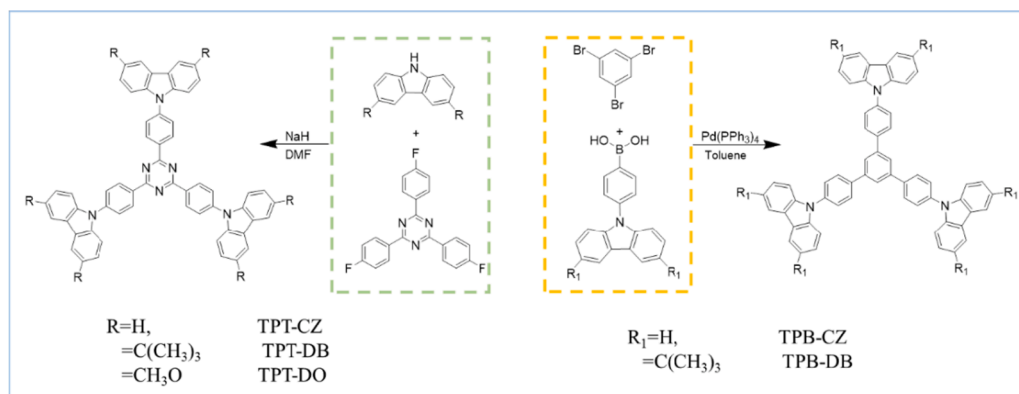
the intersystem transition (ISC), then T<sub>n</sub> undergoes relaxation and internal conversion to the first triplet-excited state (T<sub>1</sub>), which subsequently reaction with molecular oxygen to generate <sup>1</sup>O<sub>2</sub>, followed by photobleaching [18–20]. Different from inhibiting the photooxidation active site of molecules, photostability of organic materials can be significantly improved by constructing dense intermolecular stacking and strong interactions, which can reduce non-radiative transition of triplet excitons by suppressing intramolecular rotation and vibration, and formation of <sup>1</sup>O<sub>2</sub> due to the decreased oxygen diffusion rates to the luminous center [8,21]. Overall, emission intensity,  $\Delta E_{st}$  and reactive oxygen species (ROS) play an important role in affecting photostability of OFD.

Here, three s-triazine (TPT) dyes and two 1,3,5-triphenylbenzene (TPB) derivatives, named as TPT-CZ, TPT-DB, TPT-DO, TPB-CZ and TPB-DB respectively, were designed and synthesized (Scheme 1). Carbazole (CZ) are chosen as electron donor, while TPT and TPB are used as electron acceptor, forming strong and weak intramolecular charge transfer (ICT) effect respectively, and then ICT effect is further fine-tuned by changing substituents (H, OCH<sub>3</sub> and *t*-Bu) on carbazole unit. The reported literatures show that enhancing ICT effect is conducive to reduce  $\Delta E_{st}$ , but the relationship of ICT effect,  $\Delta E_{st}$ , ROS and photostability has not been investigated in detail up to now [22–24]. Combined theoretical calculation with the test of absorption, excitation, and emission spectra, AIE activity, photostability and generative capacity of <sup>1</sup>O<sub>2</sub>, intrinsic mechanisms affecting photostability of OFD are analyzed and discussed. Meanwhile, photostability of the OFD are further investigated in oxygen-free environment. According to previous method, the doping films of OFD were prepared by taking advantage of polyvinyl chloride (PVC), polybutylene adipate-polybutyrene terephthalate copolymer (PBAT), and different ethylene–vinyl alcohol copolymers (EVA) [25–26]. In contrast, oxygen isolated external environment is expected to be constructed for OFD based on amphiphilicity, and strong intramolecular and intermolecular hydrogen bonds of EVA, which remarkably enhance photostability of the OFD.

## 2. Experimental section

### 2.1. Measurement and characterization

<sup>1</sup>H NMR spectra and <sup>13</sup>C NMR spectra were obtained with a Varianova instrument at 500 MHz and 100 MHz using tetramethylsilane (TMS) as the internal standard, and CDCl<sub>3</sub>, DMSO as the solvent in all cases. UV–vis absorption spectra were obtained on a MaPada UV-3200PCS spectrophotometer. Fluorescent emission spectra were obtained on a Hitachi F-2500 fluorescence spectrophotometer. MALDI/HRMS was recorded on an UltrafleXtreme MALDI-TOF/TOF mass spectrometer (Bruker, Germany). Thermal stability was determined by thermogravimetric analyzer (TGA, SDT Q600) over a temperature range



Scheme 1. Synthetic procedures for the target compounds TPT-CZ, TPT-DB, TPT-DO, TPB-CZ and TPB-DB.

of 20–1000 °C at a heating rate of 10 °C min<sup>-1</sup> under N<sub>2</sub> atmosphere.

## 2.2. Materials

THF was dried according to standardized procedures previously described. All the other chemicals and reagents used in this study were of analytical grade without further purification. In general, all the intermediates and final compounds were purified by column chromatography on silica gel (200–300 mesh), and crystallization from analytical grade solvents. Reactions were monitored using thin layer chromatography (TLC). The synthetic methods of target compounds were shown as Scheme 1. The synthetic methods of TPT and TPB were carried out according to the reported literature [27].

## 2.3. Synthesis

### 2.3.1. 2,4,6-tris(4-(9H-carbazol-9-yl)phenyl)-1,3,5-triazine (TPT-CZ)

Under argon atmosphere, carbazole and NaH were added to a two necked round bottom flask equipped with a reflux condenser and followed by DMF. The reaction mixture was stirred for 30 min under inter condition. Afterward, 2,4,6-tris(4-fluorophenyl)-1,3,5-triazine in DMF was poured in all at once and the reaction mixture was stirred at 150 °C for overnight. The reaction was monitored by TLC, and after completion, the reaction flask was cool to room temperature. The black mixture was diluted with water and the crude product was extracted with dichloromethane. Organic phases were dried over anhydrous sodium sulphate and the solvent was removed. The crude product was purified by column chromatography on silica gel using 1:4 (dichloromethane: petroleum ether), to afford a yellow color solid (58%). <sup>1</sup>H NMR (500 MHz, CDCl<sub>3</sub>) δ 9.13 (d, *J* = 10 Hz, 1H), 8.21 (d, *J* = 5 Hz, 1H), 7.91 (d, *J* = 5 Hz, 1H), 7.63 (d, *J* = 10 Hz, 1H), 7.53–7.47 (m, 1H), 7.38 (d, *J* = 10 Hz, 1H). (Fig. S1 of the Supporting Information) HRMS (MALDI-TOF): *m/z* 805.3081 [[M + H]<sup>+</sup>, calculated 805.3080] (Fig. S2).

### 2.3.2. 2,4,6-tris(4-(3,6-ditertbutyl-9H-carbazol-9-yl)phenyl)-1,3,5-triazine (TPT-DB)

This compound was synthesized by the same method as described for TPT-CZ. A white solid was obtained in yield of 54%. <sup>1</sup>H NMR (500 MHz, Chloroform-*d*) δ 9.07 (d, *J* = 10 Hz, 1H), 8.18 (s, 1H), 7.86 (d, *J* = 10 Hz, 1H), 7.56–7.51 (m, 2H), 1.49 (s, 9H) (Fig. S3). HRMS (MALDI-TOF): *m/z* 1141.6840 [[M + H]<sup>+</sup>, calculated 1141.6836] (Fig. S4).

### 2.3.3. 2,4,6-tris(4-(3,6-dimethoxy-9H-carbazol-9-yl)phenyl)-1,3,5-triazine (TPT-DO)

This compound was synthesized by the same method as described for TPT-CZ. A yellow solid was obtained in yield of 60%. <sup>1</sup>H NMR (500 MHz, Chloroform-*d*) δ 9.08 (s, 1H), 7.86 (d, *J* = 10 Hz, 1H), 7.61 (d, *J* = 5 Hz, 1H), 7.55 (d, *J* = 10 Hz, 1H), 7.12 (dd, *J* = 10 Hz, 1H), 4.00 (s, 3H) (Fig. S5). <sup>13</sup>C NMR (100 MHz, CDCl<sub>3</sub>) δ: 168.99 (s), 155.44 (s), 143.27 (s), 136.50(s), 134.10 (s), 130.69 (s), 126.14 (s), 124.26(s), 114.82(s), 110.95 (s), 102.56 (s), 56.66 (s) (Fig. S6). HRMS (MALDI-TOF): *m/z* 1007.3531 [[M + Na]<sup>+</sup>, calculated 1007.3533] (Fig. S7).

### 2.3.4. 9,9'-(5'-(4-(9H-carbazol-9-yl)phenyl)-[1,1':3',1''-terphenyl]-4,4'-diyl)bis

(9H-carbazole) (TPB-CZ).

In a 250 mL flask were added 4-(9H-Carbazol-9-yl)phenylboronic acid (0.5168 g, 1.8 mmol), 1,3,5-tribromobenzene (0.19 g, 0.6 mmol), aqueous potassium carbonate (2 M) and toluene (15 mL), then the mixture was added Pd(PPh<sub>3</sub>)<sub>4</sub> (0.104 g, 0.09 mmol) under nitrogen at 110 °C coil bath for 24 h. After cooling to room temperature, the reaction mixture was poured into water and extracted with dichloromethane. The combined organic layers were dried over anhydrous Na<sub>2</sub>SO<sub>4</sub> and evaporated in vacuum. The crude product was purified by chromatography (silica gel; dichloromethane/petroleum = 1:5). A white solid was obtained. Yield = 80.34%. <sup>1</sup>H NMR (500 MHz, CDCl<sub>3</sub>) δ 8.19

(d, *J* = 10 Hz, 2H), 8.07–8.00 (m, 3H), 7.76 (d, *J* = 5 Hz, 2H), 7.54 (d, *J* = 10 Hz, 2H), 7.47 (t, *J* = 15 Hz, 2H), 7.33 (t, *J* = 10 Hz, 2H) (Fig. S8). HRMS (MALDI-TOF): *m/z* 824.3041 [[M + Na]<sup>+</sup>, calculated 824.3037] (Fig. S9).

### 2.3.5. 9,9'-(5'-(4-(3,6-di-tert-butyl-9H-carbazol-9-yl)phenyl)-[1,1':3',1''-terphenyl]-

4,4'-diyl) bis (3,6-di-tert-butyl-9H-carbazole) (TPB-DB).

This compound was synthesized by the same method as described for TPB-CZ. An off-white solid was obtained in yield of 83.33%. <sup>1</sup>H NMR (500 MHz, Chloroform-*d*) δ 8.29 (s, 2H), 7.95–7.90 (m, 3H), 7.76 (d, *J* = 5 Hz, 2H), 7.59 (d, *J* = 10 Hz, 2H), 7.52 (d, *J* = 10 Hz, 2H), 1.38 (s, 18H) (Fig. S10). HRMS (MALDI-TOF): *m/z* 1138.6968 [[M + H]<sup>+</sup>, calculated 1138.6973] (Fig. S11).

## 2.4. Preparation of light conversion films

Polyvinyl chloride (PVC)/polybutylene adipate-polybutylece terephthalate copolymer (PBAT) /25% ethylene-vinyl alcohol copolymers (EVA)/40% EVA (1 g) and TPT-DB (0.01 g) were dissolved into 15 mL THF in a single-necked flask, placed in ultrasonic oscillator for 3 h, and mixed evenly. Poured the mixture on a glass plate and spread it quickly with a glass rod. Finally, the films were put into a ventilated cabinet until the THF was volatilized completely, and the corresponding light conversion film of TPT-DB (1% mass fraction) including 1%PVC@film, 1%PBAT@film, 25%EVA@film (Polyvinyl alcohol accounts for 25% of the weight of EVA copolymer) and 40%EVA@film (Polyvinyl alcohol accounts for 40% of the weight of EVA copolymer) were obtained. According to this method and previously reported documents [3,26], other light conversion films were obtained.

## 3. Results and discussion

### 3.1. UV-vis absorption and fluorescent emission spectra in solutions

To investigate ICT effect of TPT-CZ, TPT-DB, TPT-DO, TPB-CZ and TPB-DB, their UV-vis absorption and fluorescent emission spectra were tested in various solvents. Fig. 1 and Table S1 show that the five dyes contain two absorption bands, located at 270–320 nm and 330–470 nm respectively. The former comes from the π-π\* transition of the TPT/TPB unit, and the latter is attributed to ICT from carbazole donor to TPT/TPB core. Generally, absorption maxima of the five dyes give a slight red shift with the increase of solvent polarity, indicating small ground state dipole moment, while emission maxima give obvious redshifts, outlining easily polarized excited states [28]. Compared with n-hexane, strength ratio between ICT and π-π\* absorption band, as well as half-width of emission maxima increased significantly in other solvents, meaning gradual transition of emission state from local state to ICT state. By comparison, absorption and emission maxima present broadly bathochromic-shift in order of TPT-DO > TPT-DB > TPT-CZ > TPB-DB > TPB-CZ in the same solvent due to increased ICT effect, which come from enhanced electron-donating ability (CH<sub>3</sub>O->C(CH<sub>3</sub>)<sub>3</sub>->H) and electron-accepting ability (TPT > TPB). As expected, these distinctions effectively achieve rough and fine adjustment of ICT effect. Furthermore, ICT effect and optical properties of the dyes are confirmed by density functional theory calculations. As shown in Fig. 2, ground-state geometries of the dyes were calculated and optimized at the B3LYP/TZVP level using the Gaussian 09 W package, and the structures and molecule orbitals (MOs) were generated by Multiwfn [29] and VMD30 [30]. The results showed the five luminophores exhibit twisted molecular configurations, whose lowest unoccupied molecular orbital (LUMO) are predominantly distributed on the TPT/TPB unit, while the highest occupied molecular orbital (HOMO) are mainly located in the carbazole moiety for TPT-CZ, TPT-DB and TPT-DO, but in both carbazole moiety and TPB unit for TPB-CZ and TPB-DB, outlining clear shifts in electron cloud density and more molecular orbital overlap for TPB-CZ and TPB-

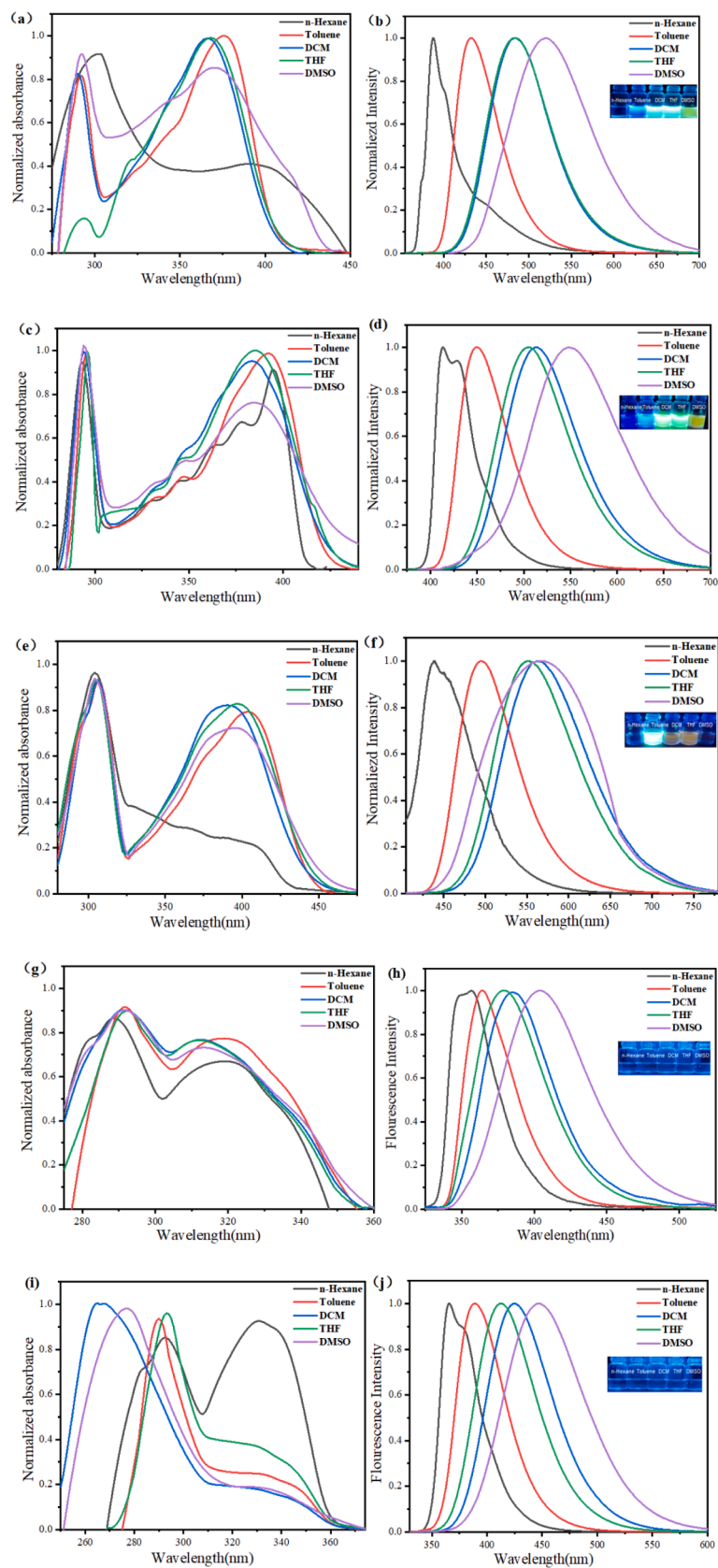


**Fig. 1.** Normalized UV-vis absorption spectra of (a) TPT-CZ, (c) TPT-DB, (e) TPT-DO, (g) TPB-CZ and (i) TPB-DB in various solvents (solution concentration: 10  $\mu$ M). Normalized fluorescence spectra of (b) TPT-CZ, (d) TPT-DB, (f) TPT-DO, (h) TPB-CZ and (j) TPB-DB in various solvents (solution concentration: 10  $\mu$ M; excitation wavelength: 369 nm, 385 nm, 398 nm, 317 nm, 340 nm, respectively; inset is the irradiation of different solvents under 365 nm UV illumination).

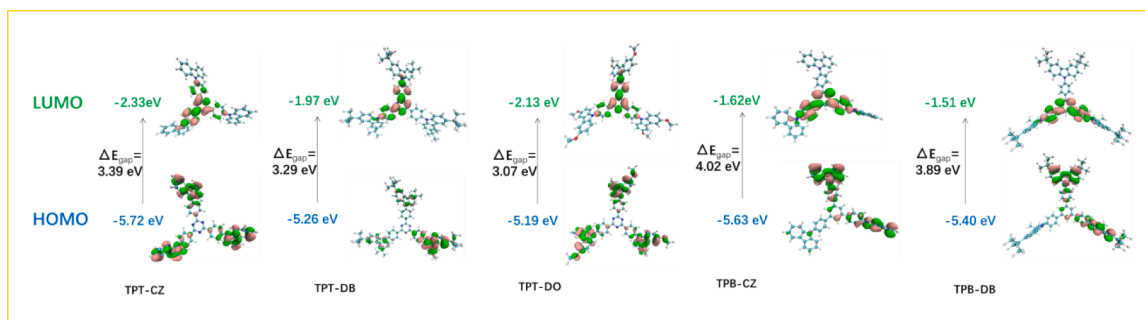


Fig. 2. Optimized geometry, HOMO and LUMO energy level diagrams for TPT-CZ, TPT-DB, TPT-DO, TPB-CZ and TPB-DB.

DB than TPT-CZ, TPT-DB and TPT-DO. Obviously, TPT-CZ, TPT-DB and TPT-DO exhibit stronger ICT effect than TPB-CZ and TPB-DB, which is consistent with the results of absorption and emission spectra test, meanwhile, discrepancy of the electron cloud density in HOMO orbitals can be easily perceived among of TPT-CZ, TPT-DB and TPT-DO. For TPT-DB, HOMO is mainly concentrated in one carbazole unit, but evenly distributed in three carbazole units for TPT-CZ and TPT-DO. With the increase of electron-donating ability of substituents, the energy gap ( $\Delta E_{\text{gap}}$ ) between HOMO and LUMO decreases in turn for TPT-CZ, TPT-DB and TPT-DO, leading to successive red-shift of fluorescence emission from TPT-CZ, TPT-DB to TPT-DO. Theoretically, introducing electron-donating group will heighten HOMO and LUMO energy level of molecules, thus it is reasonable that HOMO energy levels of TPT-CZ, TPT-DB and TPT-DO increase successively due to enhanced electron-donating ability for  $\text{H} < \text{C}(\text{CH}_3)_3 < \text{CH}_3\text{O}-$ , but abnormal for LUMO energy levels of TPT-DB in comparison with that of TPT-DO.

### 3.2. Aggregation-induced emission properties

Conventional dyes typically have strong fluorescence emission in solution, but aggregation often leads to fluorescence attenuation or quenching, which precludes their applications in light conversion agricultural film, organic electroluminescent devices, bioimaging and so on. In general, AIE-active dyes possess a twisted molecular conformation, which can suppress  $\pi-\pi$  stacking, ascribed to the key factor of aggregation-induced quenching (ACQ) [31,32]. As shown in Fig. 3a-b, the emission intensity of TPT-CZ decreases sharply until the volume fraction of water ( $f_w$ ) reaches 60%. When  $f_w$  increased from 0 to 40%, the emission maxima present continuous red shifts, which is due to increase in solvent polarity leading to enhanced non-radiation deactivation and reduced band gap. Despite emission intensity still decreases, emission maxima showed evident blue shifts at  $f_w = 50-60\%$ , which was attributed to the formation of aggregated states, moreover, aggregate particles are relatively loose, which cannot inhibit the rotation and vibration of C-C and C-N bonds, resulting in the continuous decline of fluorescence intensity. With the further increase of  $f_w$ , the enhanced and blue-shifted fluorescence emissions are simultaneously observed. When the luminophores aggregate into nanoparticles at  $f_w = 70-90\%$ , the inner nanoparticles are surrounded by the hydrophobic luminophores, which reduces the external polarity of the luminophores and suppresses molecular rotation and vibration, resulting in blue-shifted and enhanced fluorescence emission. Similar to TPT-CZ, TPT-DB and TPT-DO also experienced fluorescence quenching and enhancement, accompanied by red/blue shift of the emission maxima (Fig. 3c-f), which are dominated by increased solvent polarity and non-benign solvent-induced aggregation, respectively. Generally, TPT-CZ exhibits ACQ characteristic, while TPT-DB and TPT-DO show dual-state fluorescence emission. Combined with the above, improved fluorescent intensity in the aggregated state can be achieved by the introduction of substituent groups for TPT derivatives, which can suppress intermolecular  $\pi-\pi$  stacking due to increased steric hindrance. Different from TPT derivatives, TPB-CZ and

TPB-DB showed complex fluorescence fluctuations (Fig. 3g-j). Firstly, a decrease in emission intensity was observed for TPB-CZ as  $f_w$  increased to 10% from 0, accompanied by red shift of emission maxima, which was due to increased solvent polarity. Then, emission intensity reaches a maximum at  $f_w$  of 40%, furthermore, red shift of emission maxima indicates that enhanced emission intensity should be attributed to planarization of molecular configuration rather than formation of aggregated state. When  $f_w$  reached 50%, solvent polarity plays a leading role once again, resulting in red shift of emission maxima and decline of emission intensity. Until  $f_w$  reached 60%, emission maxima appear blue shift due to molecular aggregation, and emission intensity reaches the lowest point. Subsequently, emission intensities fall after rise under the combined action of solvent polarity and aggregation. TPB-DB show similar fluorescence emission to TPB-CZ, except for enhanced emission at  $f_w = 90\%$  due to substituent effect of  $-\text{C}(\text{CH}_3)_3$ , but both TPB-CZ and TPB-DB show ACQ characteristic. As speculation, the weak ICT effect is not conducive to the electron repulsion of TPB unit, which easily lead to  $\pi-\pi$  stacking [33,34].

### 3.3. Light-conversion quality

Choosing PVC and PBAT as film-forming substrates respectively, doping films were prepared by dissolving OFD and PVC/PBAT at a weight ratio of 1:100, various doping films named as TPT-CZ, TPT-DB, TPT-DO, TPB-CZ and TPB-DB@PVC/PBAT films. In the range of 380–780 nm, the light conversion quality of the doping films is measured and evaluated by using a HiPoint HR-450 analyzer and the blank film without dye as the control. Taking TPT-CZ as an example, Fig. 4a-d and Table S2, S4 indicates spectral intensities of TPT-CZ@PVC films are evidently lower than that of blank film before 440 nm, but spectral intensities of the doping film increased significantly from 440 nm to 780 nm. The percentage of 380–440 nm amongst the whole waveband indicates 4.35% reduction for the doping film than the blank film, but an increase of 0.82%, 1.08%, 1.43% and 1.02% for 440–500 nm, 500–600 nm, 600–700 nm and 700–780 nm wavebands in turn. which confirms TPT-CZ not only converts ultraviolet light and partially blue light but also significantly improve transmittance of PVC film, which is further verified by excitation spectrum (Fig. S16a) and emission spectra (Fig. S17a). Fig. S16a shows TPT-CZ has a wide excitation band from 280 nm to 455 nm in PVC film, and exhibits excitation dependent fluorescence emission, whose emission maxima shifts to 500 nm from 440 nm with the increase of excitation wavelength, even fluorescence emission wavelength can cover up to 660 nm (Fig. S17a), thereby significantly elevated yellow-green light intensity (500–600 nm) can be attributed to the larger conjugated structure of TPT-CZ, but for near infrared wavelengths (700–780 nm) ascribed to improved transmittance, for red wavelengths (600–700 nm), which should come from combined action of excitation dependent fluorescence emission and improved transmittance. By contrast, the photosynthetic photon flux density (PPFD) of the doping film is close to that of the blank film at 400–500 nm, but PPFD of the doping film increased up to 19.62%

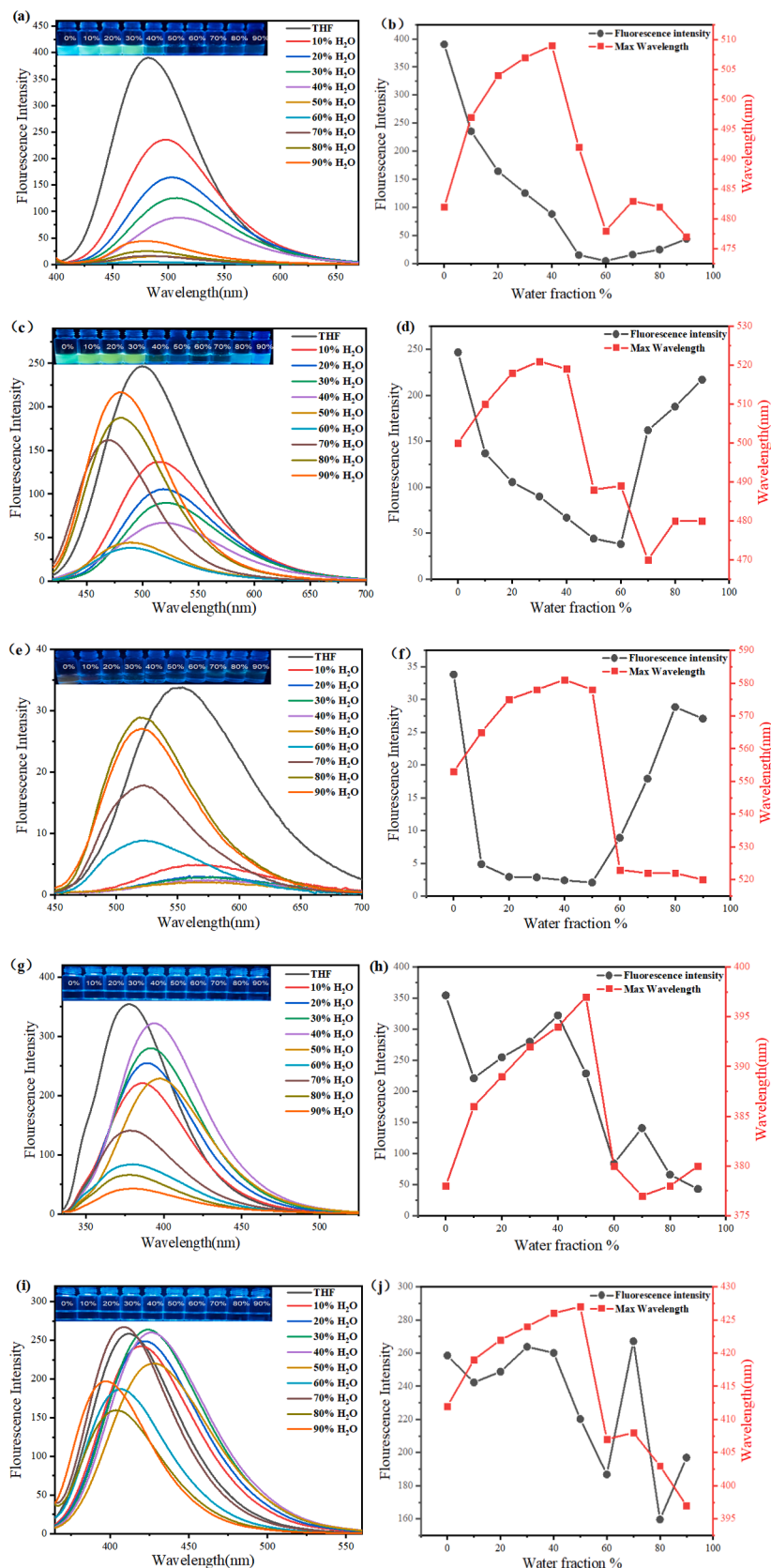


**Fig. 3.** Fluorescence emission spectra of (a) TPT-CZ, (c) TPT-DB, (e) TPT-DO, (g) TPB-CZ and (i) TPB-DB in THF/H<sub>2</sub>O mixtures with different water contents (solution concentration: 10 μM; excitation wavelength: 369 nm, 385 nm, 398 nm, 312 nm, 337 nm, respectively). Fluorescence emission peak intensity, maximum emission wavelength and water fraction of (b) TPT-CZ, (d) TPT-DB, (f) TPT-DO, (h) TPB-CZ and (j) TPB-DB. Solution concentration: 10 μM. (inset: images in THF/water mixtures with different fractions of water under 365 nm UV illumination).

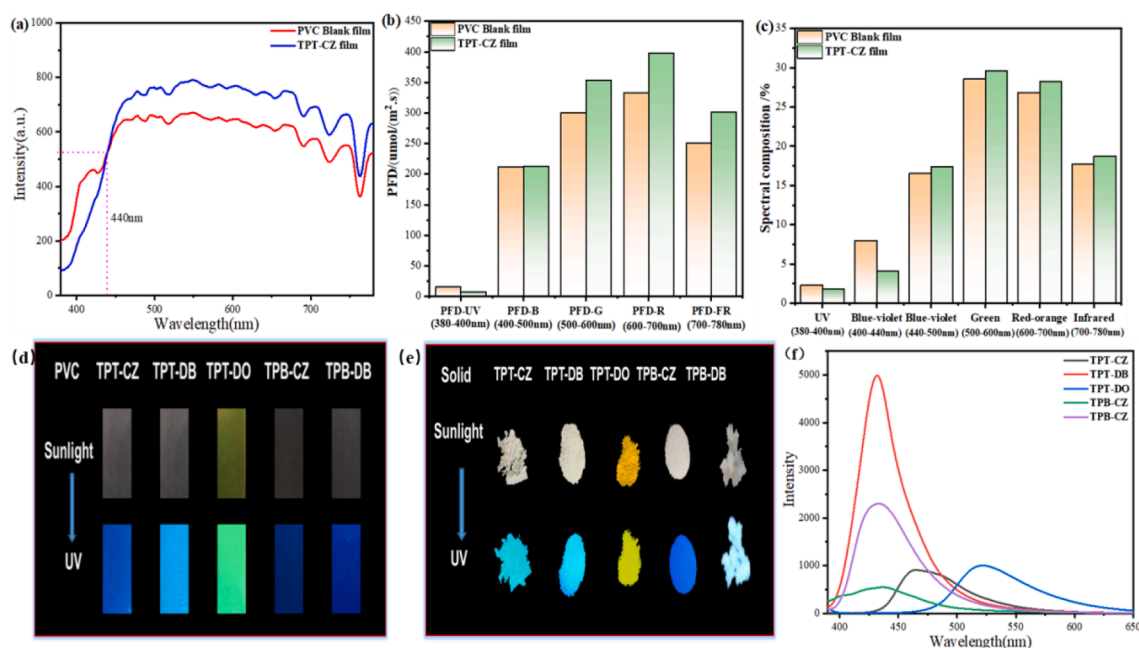


**Fig. 4.** (a) Light quality measured under blank and TPT-CZ@PVC film; (b) PFD of UV, visible and infrared light of blank and TPT-CZ@PVC film; (c) UV, visible and infrared light compositions of blank and TPT-CZ@PVC film; (d) different PVC doped films under sunlight and UV light irradiation; (e) photograph of the luminogens in solid-state under sunlight and UV light irradiation; (f) Solid-state fluorescence spectra of the luminogens (excitation wavelength: 369 nm, 385 nm, 398 nm, 317 nm, 340 nm, respectively).

compared with that of blank film at 600–700 nm, which will have a significant effect on promoting crop growth. By comparison, the intersection points of intensity curve between doping film and blank film are located at 457 nm for TPT-DO, showing obviously red shift relative to TPT-CZ due to  $-OCH_3$  with increased electron-donating ability, which further lead to reduction of PFD at 400–500 nm (Fig. S12 and Table S2, S4). However, Fig. S13 and Table S5 indicate the spectral curves of TPB-CZ@PVC and TPB-DB@PVC films almost overlap with that of blank PVC film, meaning weak light conversion performance. In general, TPT-DB showed the best light conversion performance, whose PFD at

400–500 nm and 600–700 nm in doping film increased successively to 6.20% and 25.78% of the blank film, while PFD at 380–400 nm reduced by 81.23%. Compared with TPB-CZ@PVC film, TPB-DB@PVC film shows higher PFD in the whole waveband of 400–780 nm. Furthermore, Fig. 4f shows TPT-DB and TPB-DB with *tert*-butyl groups, which show the strongest fluorescence emission in solid state. From that, we conclude that *tert*-butyl group with large space conformation can reduce intermolecular interactions, which is conducive to enhance fluorescence emission in aggregated state, solid state and doping film. Figs. S14–15 show five dyes have similar light conversion performance in PBAT films,

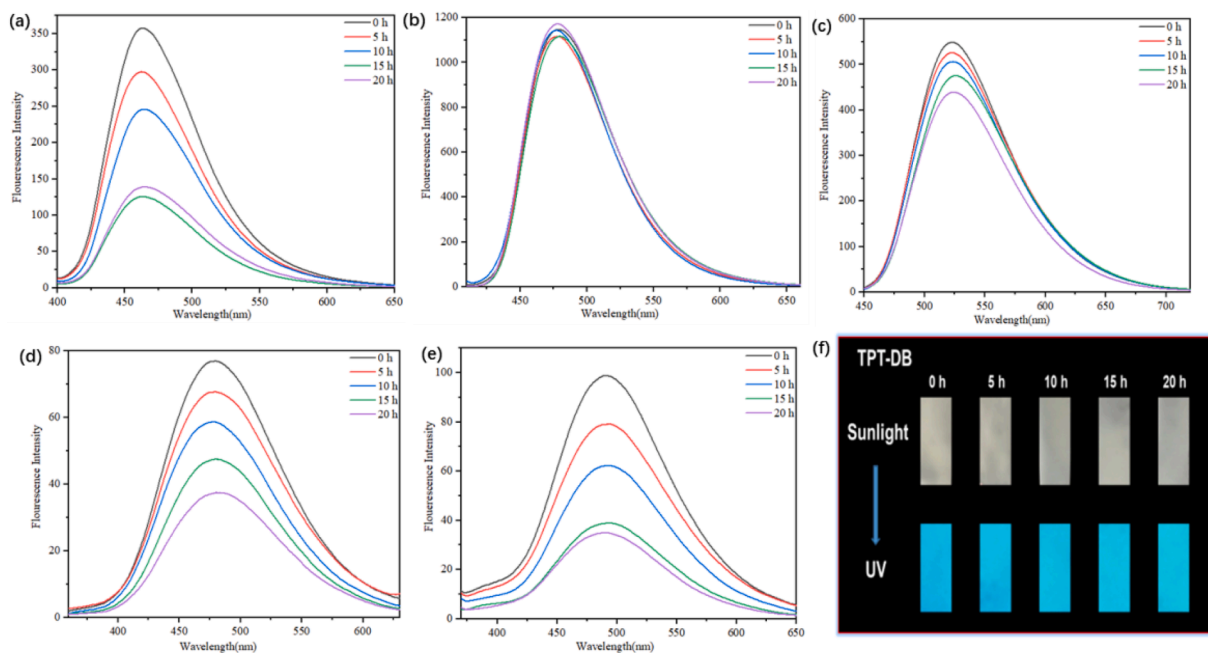


**Fig. 5.** Emission spectra of (a) TPT-CZ, (b) TPT-DB, (c) TPT-DO, (d) TPB-CZ and (e) TPB-DB@PBAT films; and (f) photograph of TPT-DB@PBAT film at different radiation times (excitation wavelength: 369 nm, 385 nm, 398 nm, 317 nm, 340 nm, respectively).

but increased polarity compared with PVC matrix leads to red-shift of spectral intersection between doping film and blank film (Figs. S16, S17 and Table S6, S7).

### 3.4. Photostability and thermal stability

By intensified photodegradation of ultraviolet light radiation (365 nm, 40 w), photostability of five dyes was investigated in PBAT films. As shown in Fig. 5 and S18, emission maxima of five dyes remained stable without perceptible wavelength shift, but fluorescence intensity decay forms a strong contrast. Among of five dyes, TPT-DB shows the best photostability, its fluorescence intensity remains 93.4% of the initial value after UV radiation of 20 h, while fluorescence intensities of TPT-CZ, TPT-DO, TPB-CZ and TPB-DB are maintained at 34.5%, 77.8%, 48.7% and 34.7% of the initial value respectively. To find out the key factors of affecting photostability, the excited state behaviors of TPT-CZ, TPT-DB and TPT-DO were investigated by density functional theory (DFT) and time-dependent density functional theory (TD-DFT) at the M062X [35]/def2SVP [36] level using the Gaussian 16 package [37]. The TD-DFT calculations for all molecules were performed using the optimized  $S_0$  geometry. The orbital coupling constant ( $\xi$ ) was determined at the M062X/def2SVP level using on ORCA 4.2.1 [38]. The  $\xi$  was calculated using the optimized  $S_0$  geometry, and the detailed topological analysis were performed using the Multiwfn program [28]. It can be seen from Fig. S19 that the  $S_1$  of the single-molecule state of TPT-CZ, TPT-DB, TPT-DO are 3.748 eV (331 nm), 3.625 eV (342 nm) and 3.507 eV (352 nm) in turn, whose order is consistent with the experimental result. The corresponding energy gaps between  $S_1 \rightarrow T_1$  are 0.594 eV, 0.562 eV and 0.449 eV respectively. What's more, the closer energy gaps and larger  $\xi$  between  $S_1$  and  $T_1$ , which is convenient for promoting intersystem transitions and the generation of triplet excitons, thereby TPT-CZ, TPT-DB and TPT-DO have the ability to form reactive oxygen in theory. By contrast, TPT-DB with large  $\xi$  should have the strongest ability to generate reactive oxygen species, followed by TPT-CZ and TPT-DO. 2', 7'-dichlorodihydrofluorescein diacetate (DCFH-DA) was used as an indicator of reactive oxygen. The indicator is non-fluorescent, but it can emit bright fluorescence when triggered by

reactive oxygen. As shown in Fig. S20, the emission intensity of the control group (DCFH-DA + PBS solution, concentration of  $1 \times 10^{-5}$  mol  $L^{-1}$ ) was low within 30 min of visible light irradiation. Under the same conditions, an equal volume of dyes solution was used instead of PBS, and then the fluorescence intensity was measured by using fluorescence spectrometer ( $\lambda_{ex} = 480$  nm,  $\lambda_{em} = 527$  nm). The production of reactive oxygen species can be indirectly quantified by comparing the fluorescence intensity between the control and experimental groups. The results showed that the fluorescence intensities of the DCFH-DA solution containing five different light conversion agents were higher than that of the blank group, clearly showing that all five dyes have the ability of generating reactive oxygen under illumination, moreover, reactive oxygen generation capacity of three TPT derivatives is in good agreement with the above theoretical calculation, but there is no definite rule to be summarized between photostability (TPT-DB, TPT-DO, TPB-CZ, TPB-DB and TPT-CZ), reactive oxygen generation capacity (TPT-DB, TPB-DB, TPT-CZ, TPT-DO and TPB-CZ) and ICT effect (TPT-DO, TPT-DB, TPT-CZ, TPB-DB and TPB-CZ). The mechanism studies demonstrated that the influencing factors of photostability are complex. To completely inhibit the production of  $^1O_2$  and other reactive oxygen species, photostability of five dyes are further investigated in an oxygen-free environment by vacuum degassing and argon replacement, unexpectedly, five dyes all show excellent photostability in PBAT-doped films, whose fluorescence emission intensities only give small fluctuations (Fig. 6 and S21). Obviously, constructing oxygen-free environment will become the most important measure to enhance the photostability of organic light conversion agents.

To reduce the oxygen content around room temperature phosphorescence (RTP) molecules, polyvinyl alcohol is often used as a doping matrix to block the diffusion of oxygen, which greatly improves the phosphorescence life of RTP materials. Inspired by this, the doping film of TPT-CZ is prepared by choosing amphiphatic EVA, in which TPT-CZ and hydrophobic polyethylene have excellent compatibility, facilitating the uniform dispersion of fluorescent dyes, while hydrophilic polyvinyl alcohol can form intramolecular/intermolecular hydrogen bonding and a rigid external environment, inhibiting oxygen diffusion to inside the light conversion film. Moreover, the doping films with

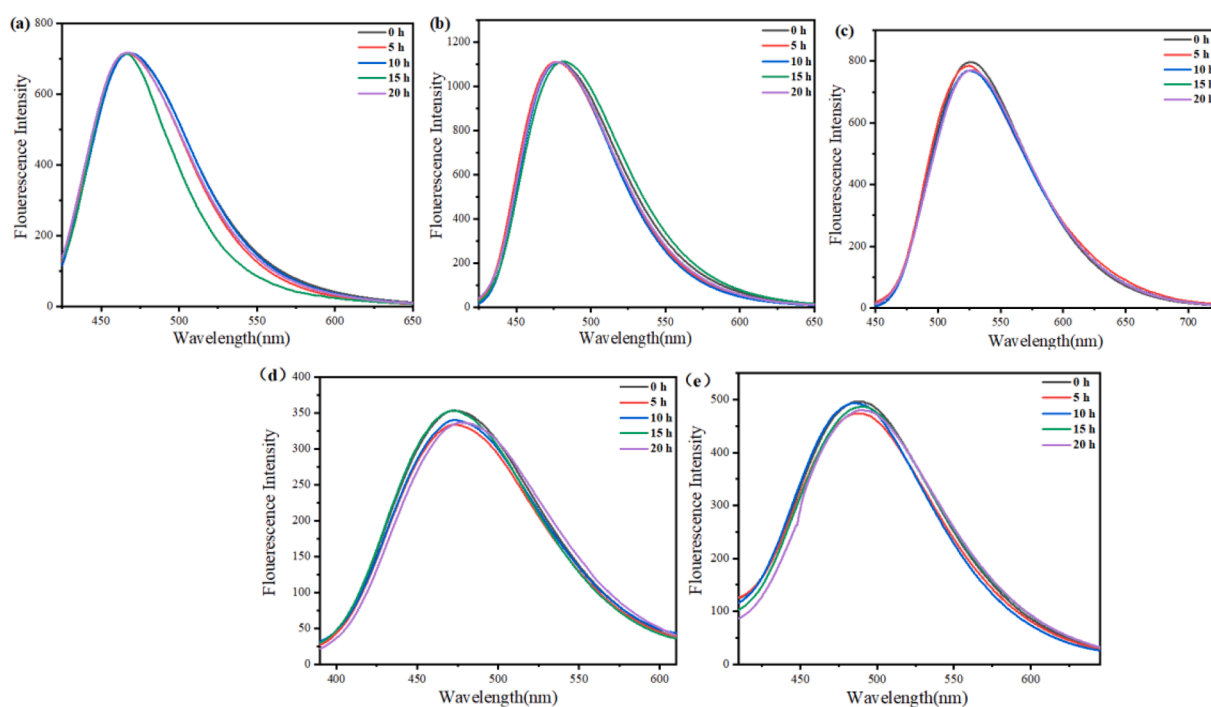


Fig. 6. Emission spectra of (a) TPT-CZ, (b) TPT-DB, (c) TPT-DO, (d) TPB-CZ and (e) TPB-DB@PBAT films in oxygen-free environment for different irradiation times (excitation wavelength: 369 nm, 385 nm, 398 nm, 317 nm, 340 nm, respectively).

different polyvinyl alcohol content are investigated to further explore the relationships between photostability of light conversion film and polyvinyl alcohol content. The results indicate 25% (TPT-CZ@25%EVA film) and 40% (TPT-CZ@40%EVA film) doping films (weight ratio of polyvinyl alcohol in copolymer) are easy to prepare, but not for 10% doping film due to poor solubility. Furthermore, the excitation and emission spectra of two doping films are tested, and the corresponding photostability is discussed in detail. Fig. 7a show TPT-CZ@40%EVA film presents wider half of the maximum excitation peak compared with that of TPT-CZ@25%EVA film, which may be due to better dispersion in former than the latter, and thereby lead to stronger emission intensity and more matching emission peak with crop absorption. With the extension of ultraviolet radiation time, emission intensities of the two light-conversion films remain roughly unchanged, indicating outstanding photostability (Fig. 7b, c). To sum up, both TPT-CZ@25%EVA and TPT-CZ@40%EVA films can significantly enhance photostability of TPT-CZ, which is expected to break the bottleneck of OFD as light conversion agents.

The above results indicates that TPT-DB can be appointed as the highly efficient blue-violet light conversion agent. Furthermore, thermal stability of the light conversion agents is an important evaluating indicator, thereby the thermal gravimetric analysis (TGA) of TPT-DB was investigated. As shown in Fig. 8, the thermal decomposition of TPT-DB can be divided into two stages. The initial decomposition temperature of TPT-DB is 184 °C, according to weight loss, the first stage presents a slow slope line between 185 °C and 646 °C, and this stage removes  $-C(CH_3)_3$ . Second stages occur between 647 °C and 768 °C, this rapid decomposition should be the result of decomposition, oxidation, and combustion. Generally, TPT-DB can meet the application requirements of light conversion agents, the higher initial decomposition temperature and up to 374 °C Td (defined as the temperature at which a sample loses its 5% weight) indicate that TPT-DB has excellent thermal stability.

#### 4. Conclusions

In summary, TPT-CZ, TPT-DB, TPT-DO, TPB-CZ and TPB-DB with different push-pull electronic system were designed and synthesized, and characterized and confirmed by  $^1H$  NMR,  $^{13}C$  NMR and HR-MS. The absorption and emission spectra of five OFD indicate that rough-tune and fine-tune of ICT effect were successfully achieved, which is further confirmed by theoretical calculation. AIE experiments and fluorescence emission spectra confirmed that  $-C(CH_3)_3$  with large steric

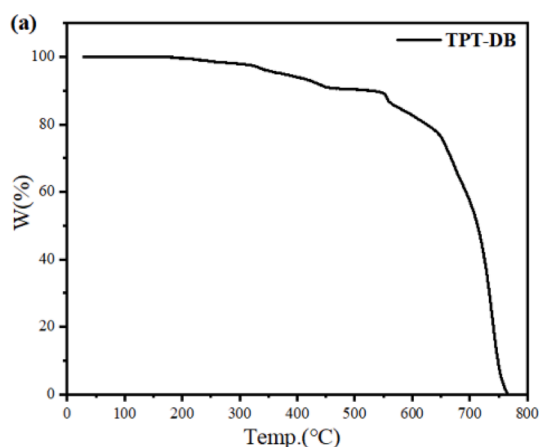


Fig. 8. TGA thermograms of (a) TPT-DB recorded under nitrogen atmosphere at 10 °C min<sup>-1</sup> scan rates.

resistance is advantageous to enhance solid-state fluorescence emission of OFC, thereby TPT-DB film shows the strongest fluorescence emission and the best light conversion performance. Light conversion quality further indicates that TPT-DB can not only convert ultraviolet light, but also significantly enhance the transmittance of PBAT, whose photosynthetic photon flux density at 400–500 nm and 600–700 nm increased successively to 6.20% and 25.78% of the blank film. Under intensified ultraviolet radiation (365 nm, 40 w) of 20 h, emission intensity of TPT-DB can maintain 93.4% of the initial value, exhibiting excellent photostability, and has good thermal stability with Td up to 374 °C, but it is difficult for constructing the relationships of photostability, ICT effect, reactive oxygen generation capacity and  $\Delta E_{ST}$  based on theoretical calculation and experimental test, which indicate that the factors affecting photostability are complex. Under oxygen-free conditions, fluorescence intensities of all the doping films remain stable after 20 h of irradiation, which illustrate inhibiting oxygen diffusion is very important to improve the photostability of light conversion agents. Finally, amphipathic EVA copolymer provides a simple and effective way to improve the photostability of OFD, which will accelerate the wide application of OFD as light conversion agents. Meanwhile, TPT-DB is expected to become a potential light conversion agent based on excellent photostability and fluorescence emission in the doping film.

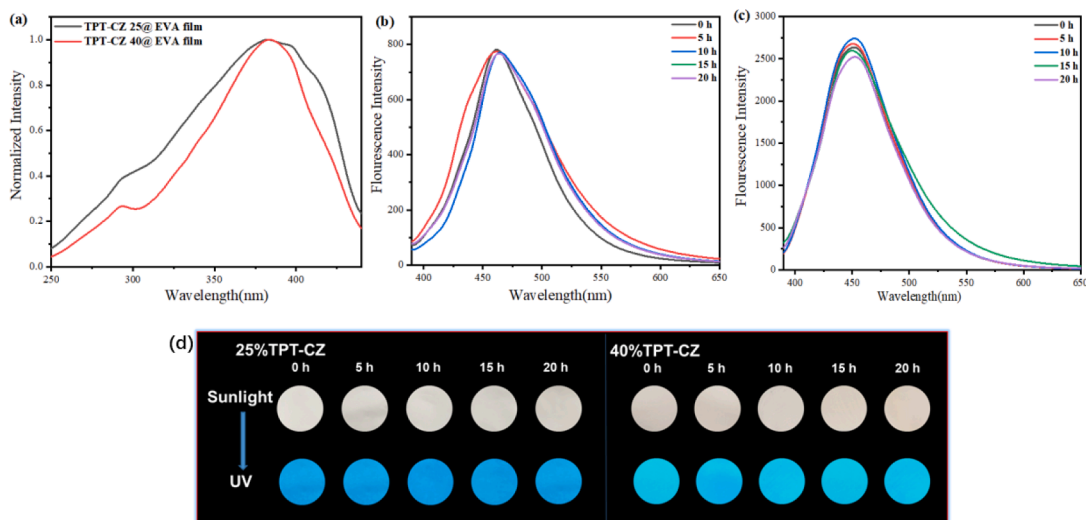


Fig. 7. Excitation spectra of (a) TPT-CZ@25%EVA and TPT-CZ@40%EVA films. Emission spectra of (b) TPT-CZ@25%EVA and (c) TPT-CZ@40%EVA films at different irradiation times (excitation wavelength: 383 nm). Photograph of (d) TPB-DB@PBAT of TPT-CZ@25%EVA and TPT-CZ@40%EVA films at different irradiation times.

## Declaration of Competing Interest

The authors declare that they have no known competing financial interests or personal relationships that could have appeared to influence the work reported in this paper.

## Data availability

Data will be made available on request.

## Acknowledgment

This work was supported by the Guangxi Natural Science Foundation (Grant No. 2020GXNSFAA159147), the National Natural Science Foundation of China (Grant No. 21766030 and 21566034) and the Guilin University of Technology Research Fund (Grant No. GUTQDJJ2019038 and GUTQDJJ2018052).

## Appendix A. Supplementary material

Supplementary data to this article can be found online at <https://doi.org/10.1016/j.saa.2022.122161>.

## References

- W. Wu, Z. Zhang, R. Dong, G. Xie, J. Zhou, K. Wu, H. Zhang, Q. Cai, B. Lei, Characterization and properties of a  $\text{Sr}_2\text{Si}_5\text{N}_8:\text{Eu}^{2+}$ -based light-conversion agricultural film, *J. Rare Earths*. 38 (2020) 45–539, <https://doi.org/10.1016/j.jre.2020.01.020>.
- Z. Zhang, Z. Zhao, Y. Lu, D.i. Wang, C. Wang, J. Li, One-step synthesis of  $\text{Eu}^{3+}$ -modified cellulose acetate film and light conversion mechanism, *Polymers*. 13 (1) (2021) 113, <https://doi.org/10.3390/polym13010113>.
- Y. Yu, Y. Wang, W. Liu, X. Jia, L. Ma, L. Ren, M. Xue, X. Liu, Exploration of highly efficient light conversion agents for agricultural film based on the bay-substituted perylene diimides derivatives, *Dyes Pigment*. 159 (2018) 90–483, <https://doi.org/10.1016/j.dyepig.2018.07.015>.
- Y. Wang, Z. Qian, X. Li, A. Qin, Y. Guo, B. Tang, Exploration of high-performance light-conversion agents based on cyanostilbene and phenanthrenecarbonitrile backbones: E/Z and position isomerism, high-contrast Michael addition reaction activity and intramolecular photocyclization, *J. Mater. Chem. C*. 9 (2021) 93–12681, <https://doi.org/10.1039/D1TC02405A>.
- D.i. Wang, H. Wang, B. Qian, H. Zou, K. Zheng, X. Zhou, Y. Song, Y.e. Sheng, Preparation of hydrophobic calcium carbonate phosphors and its application in fluorescent films, *J. Lumines*. 219 (2020) 116844, <https://doi.org/10.1016/j.jlumin.2019.116844>.
- Y. Liu, Z. Gui, J. Liu, Research progress of light wavelength conversion materials and their applications in functional agricultural films, *Polymers*. 14 (2022) 851, <https://doi.org/10.3390/polym14050851>.
- N.B. Adams, C.J. Marklew, A.A. Brindley, C.N. Hunter, J.D. Reid., Characterization of the magnesium chelatase from *Thermosynechococcus elongatus*, *Biochem J*. 457 (2014) 70–163, <https://doi.org/10.1042/bj20130834>.
- Y. Qi, Y. Wang, Y. Yu, Z. Liu, Y. Zhang, Y. Qi, C. Zhou, Exploring highly efficient light conversion agents for agricultural film based on aggregation induced emission effects, *J. Mater. Chem. C*. 4 (2016) 7–11291, <https://doi.org/10.1039/c6tc04215e>.
- Y. Wang, Y. Yu, W. Liu, L. Ren, G. Ge, Exploration of highly efficient blue-violet light conversion agents for an agricultural film based on structure optimization of triphenylacrylonitrile, *J. Agric. Food Chem*. 66 (2018) 302–13295, <https://doi.org/10.1021/acs.jafc.8b05453>.
- G. Jones, W.R. Bergmark, W.R. Jackson, Products of photodegradation for coumarin laser dyes, *Opt Commun*. 50 (5) (1984) 320–323, [https://doi.org/10.1016/0030-4018\(84\)90176-7](https://doi.org/10.1016/0030-4018(84)90176-7).
- Q. Zheng, L.D. Lavis, Development of photostable fluorophores for molecular imaging, *Curr. Opin Chem. Biol*. 39 (2017) 32–38, <https://doi.org/10.1016/j.cbpa.2017.04.017>.
- S. Moi, B. Hosamani, K. Kumar, S. Gunaga, S. Raghothama, K.H. Gowd, Photochemical studies of new synthetic derivatives of avobenzene under sunlight using UV-spectroscopy, *J. Photochem. Photobiol. A-Chem*. 420 (2021) 113488, <https://doi.org/10.1016/j.jphotochem.2021.113488>.
- S. Zhang, H. Chen, L. Wang, C. Liu, L. Liu, Y. Sun, X.C. Shen, A simple strategy for simultaneously enhancing photostability and mitochondrial-targeting stability of near-infrared fluorophores for multimodal imaging-guided photothermal therapy, *J. Mater. Chem. B*. 9 (2021) 95–1089, <https://doi.org/10.1039/D0TB02674C>.
- L. Wang, Y. Qian, Two effective strategies to improve SOCT-ISC type photosensitizers: triphenylamine BODIPY with A-D-A configuration and AIE effect and its application in A-549 cells and zebrafish, *Dyes Pigment*. 198 (2022), <https://doi.org/10.1016/j.dyepig.2021.110018>.
- F. Li, T. Zhe, K. Ma, R. Li, M. Li, Y. Liu, Y. Cao, Wang, A Naturally derived nanocomposite film with photodynamic antibacterial activity: new prospect for sustainable food packaging, *ACS Appl. Mater. Interfaces*. 13 (2021) 3008–52998, <https://doi.org/10.1021/acsmi.1c12243>.
- A. Bera, D. Bagchi, S.K. Pal, Improvement of photostability and nir activity of cyanine dye through nanohybrid formation: key information from ultrafast dynamical studies, *J. Phys. Chem. A*. 123 (35) (2019) 7550–7557, <https://doi.org/10.1021/acs.jpca.9b04100>.
- D. Chen, Q. Xu, W. Wang, J. Shao, W. Huang, X. Dong, Dong, Type I Photosensitizers Revitalizing Photodynamic Oncotherapy, *Small*. 17 (31) (2021) 2006742, <https://doi.org/10.1002/sml.202006742>.
- E.R. Sauv e, C.M. Tonge, Z.M. Hudson, Deep-blue fluorophores with imidazoacridine acceptors: enhancing photostability and two-photon fluorescence using structural constraint, *J. Mater. Chem. C*. 9 (2021) 72–4164, <https://doi.org/10.1039/D0TC05241H>.
- H.S. Lee, H.G. Song, H. Jung, M.H. Kim, C. Cho, J.-Y. Lee, S. Park, H.-J. Son, H.-J. Yun, S.-K. Kwon, Y.-H. Kim, B. Kim, Effects of backbone planarity and tightly packed alkyl chains in the donor-acceptor polymers for high photostability, *Macromolecules*. 49 (2016) 56–7844, <https://doi.org/10.1021/acs.macromol.6b01580>.
- Z. Liu, Y. Yang, Z. Sun, C. Wu, Wu, Enhanced single-particle brightness and photostability of semiconductor polymer dots by enzymatic oxygen scavenging system, *Opt. Mater*. 62 (2016) 1–6, <https://doi.org/10.1016/j.optmat.2016.09.046>.
- L. Zou, S. Guo, H. Lv, F. Chen, L. Wei, Y. Gong, Y. Liu, C. Wei, Molecular design for organic luminogens with efficient emission in solution and solid-state, *Dyes Pigment*. 198 (2022), 109958, <https://doi.org/10.1016/j.dyepig.2021.109958>.
- Z. Zhou, X. Wang, J. Chen, J. Xu, Xu, Direct observation of an intramolecular charge transfer state in epigenetic nucleobase N6-methyladenine, *Phys Chem Chem Phys*. 21 (13) (2019) 6878–6885, <https://doi.org/10.1039/C9CP00325H>.
- D. Jana, S. Jana, Donor-pyrene-acceptor distance-dependent intramolecular charge-transfer process: a state-specific solvation preferred to the linear-response approach, *ACS Omega*. 5 (2020) 56–9944, <https://doi.org/10.1021/acsomega.0c00265>.
- E. Ravindran, N. Somanathan, Somanathan, Efficient white-light emission from a single polymer system with “spring-like” self-assemblies induced emission enhancement and intramolecular charge transfer characteristics, *J. Mater. Chem. C*. 5 (19) (2017) 4763–4774, <https://doi.org/10.1039/C7TC01036B>.
- M.F. Abd Elkader, M.S. Almogbel, M.T. Elabbasy, Elabbasy, Survival and reduction in foodborne bacteria using methyl cellulose film doped with europium oxide nanoparticles, *Food Sci Nutr*. 8 (1) (2020) 291–298, <https://doi.org/10.1002/fsn3.1305>.
- Y. Ren, Z. Chen, H. Du, L. Fang, X. Zhang, Zhang, Preparation and Evaluation of Modified Ethylene-Vinyl Acetate Copolymer as Pour Point Depressant and Flow Improver for Jiangnan Crude Oil, *Ind. Eng. Chem. Res*. 56 (39) (2017) 11161–11166, <https://doi.org/10.1021/acs.iecr.7b02929>.
- S. Kumar, Y.-Y. Ma, A. Khan, Y.i. Yuan, S.-Y. Yang, Z.-Q. Jiang, M.-K. Fung, L.-S. Liao, Structurally controlled singlet-triplet splitting for blue star-shaped thermally activated delayed fluorescence emitters incorporating the tricarbazoles-triazine motifs, *Org. Electron*. 84 (2020) 105783, <https://doi.org/10.1016/j.orgel.2020.105783>.
- Y.E. Begantsova, E.V. Baranov, S.A. Chesnokov, 4-(1H-Imidazo[4,5-f][1,10]phenanthrolin-2-yl)benzaldehyde as a probe in pure solvents: Solvatochromism, electric dipole moment and pH influence, *Spectrochim. Acta. Part A: Mol. Biomol. Spectrosc*. 280 (2022) 121480, <https://doi.org/10.1016/j.saa.2022.121480>.
- T. Lu, F. Chen, Multiwfn: a multifunctional wavefunction analyzer, *J. Comput. Chem*. 33 (2012) 92–580, <https://doi.org/10.1002/jcc.22885>.
- W. Humphrey, A. Dalke, K. Schulten, Schulten, VMD: Visual molecular dynamics, *J. Mol. Graph*. 14 (1) (1996) 33–38, [https://doi.org/10.1016/0263-7855\(96\)00018-5](https://doi.org/10.1016/0263-7855(96)00018-5).
- Y. Liu, J. Hou, Y. Zhang, Y. Wang, A simple AIE chemosensor based on diphenyl imidazole scaffold for 2,4,6-trinitrophenol detection and dye absorption, *Spectrochim. Acta. Part A: Mol. Biomol. Spectrosc*. 285 (2023), 121867, <https://doi.org/10.1016/j.saa.2022.121867>.
- K. Prabakaran, R. Manivannan, Y.-A. Son, Highly emissions of TPA-linear based pyrazine derivatives with different mechanochromic luminosity, *Spectrochim. Acta. Part A: Mol. Biomol. Spectrosc*. 285 (2023), 121874, <https://doi.org/10.1016/j.saa.2022.121874>.
- J. Yang, X. Zhen, B. Wang, X. Gao, Z. Ren, J. Wang, Y. Xie, J. Li, Q. Peng, K. Pu, Z. Li, The influence of the molecular packing on the room temperature phosphorescence of purely organic luminogens, *Nat. Commun*. 9 (2018) 840, <https://doi.org/10.1038/s41467-018-03236-6>.
- Y. Wang, Z. Qian, X. Li, A. Qin, Y. Guo, B. Tang, Polymorphism and light conversion properties of anthracene-based isomers, *Dyes Pigment*. 197 (2022), 109888, <https://doi.org/10.1016/j.dyepig.2021.109888>.
- Y. Zhao, D.G. Truhlar, The M06 suite of density functionals for main group thermochemistry, thermochemical kinetics, noncovalent interactions, excited states, and transition elements: two new functionals and systematic testing of four M06-class functionals and 12 other functionals, *Theor. Chem. Account*. 120 (2008) 41–215, <https://doi.org/10.1007/s00214-007-0310-x>.
- F. Weigend, R. Ahlrichs, Ahlrichs, Balanced basis sets of split valence, triple zeta valence and quadruple zeta valence quality for H to Rn: design and assessment of

- accuracy, *Phys. Chem. Chem. Phys.* 7 (18) (2005) 3297, <https://doi.org/10.1039/B508541A>.
- [37] M. Frisch, G. Trucks, H. Schlegel, G. Scuseria, M. Robb, J. Cheeseman, G. Scalmani, V. Barone, G. Petersson, H. Nakatsuji, Gaussian 16 Revision A. 03. Gaussian Inc, Wallingford CT. 2 (2016) 4.
- [38] F. Neese, Software update: the ORCA program system, version 4.0, *Wiley Interdiscip. Rev. Comput. Mol. Sci.* 8 (2018) e1327, <https://doi.org/10.1002/wcms.1327>.